Check for updates

ARTICLE

Silencing KCC2 in mouse dorsal hippocampus compromises spatial and contextual memory

Clémence Simonnet[1,2,3,5], Manisha Sinha[1,2,3], Marie Goutierre[1,2,3], Imane Moutkine[1,2,3], Stéphanie Daumas[2,4] and Jean Christophe Poncer [1,2,3 ✉]

Delayed upregulation of the neuronal chloride extruder KCC2 underlies the progressive shift in GABA signaling polarity during development. Conversely, KCC2 downregulation is observed in a variety of neurological and psychiatric disorders often associated with cognitive impairment. Reduced KCC2 expression and function in mature networks may disrupt GABA signaling and promote anomalous network activities underlying these disorders. However, the causal link between KCC2 downregulation, altered brain rhythmogenesis, and cognitive function remains elusive. Here, by combining behavioral exploration with in vivo electrophysiology we assessed the impact of chronic KCC2 downregulation in mouse dorsal hippocampus and showed it compromises both spatial and contextual memory. This was associated with altered hippocampal rhythmogenesis and neuronal hyperexcitability, with increased burst firing in CA1 neurons during non-REM sleep. Reducing neuronal excitability with terbinafine, a specific Task-3 leak potassium channel opener, occluded the impairment of contextual memory upon KCC2 knockdown. Our results establish a causal relationship between KCC2 expression and cognitive performance and suggest that non-epileptiform rhythmopathies and neuronal hyperexcitability are central to the deficits caused by KCC2 downregulation in the adult mouse brain.

INTRODUCTION

Fast inhibitory synaptic transmission in the central nervous system relies on chloride conductance associated with both GABAA and glycine receptors. Whereas most cell types display high intracellular chloride concentration ($[Cl]_i$), mature neurons maintain much lower $[Cl]_i$ and thereby ensure a hyperpolarizing chloride influx upon GABAA or glycine receptor activation [1]. This property is supported by the expression of a neuron-specific chloride extruder, the potassium-chloride co-transporter KCC2. Early expression of the sodium-potassium-chloride cotransporter NKCC1, a ubiquitous chloride importer, and delayed upregulation of KCC2 expression combine to produce a developmental shift in neuronal $[Cl]_i$ and, consequently, in the polarity of GABA signaling in the developing CNS, from excitatory to inhibitory or shunting [1–3].

However, in the mature brain, KCC2 may be downregulated in a variety of pathological conditions, including brain trauma [4, 5], stroke [6], stress [7, 8], epilepsy [9–12] as well as schizophrenia [13–15] and autism spectrum disorders [16–19]. Most of these disorders are associated with cognitive impairment, including episodic and working memory deficits [20–23]. However, whether and how KCC2 downregulation in pathology may contribute to memory deficits has remained unexplored.

Downregulated KCC2 expression is classically thought to cause a pathological shift in the polarity of GABA signaling, from inhibitory to excitatory. Thus, depolarizing GABAA receptor-mediated responses are observed in most aforementioned conditions. Such excitatory actions of GABA in mature neuronal networks may then promote anomalous network activities underlying pathological symptoms [11, 17, 24–26]. However, KCC2 downregulation may also affect neuronal function independent of GABA signaling. KCC2 was shown to regulate activity-dependent synaptic delivery of AMPA receptors through interaction with actin-related protein partners [27–30], thereby gating long term potentiation induction [3, 27, 31]. In addition, KCC2 was shown to control membrane trafficking of leak potassium channels Task-3 through molecular interaction. KCC2 knockdown therefore induces neuronal hyperexcitability in the dentate gyrus by reducing Task-3 channel membrane expression and function [32]. These effects may combine to perturb both long term synaptic plasticity and cortical rhythmogenesis, two processes critically involved in hippocampus-dependent memory encoding and consolidation [33–36].

Here we tested whether KCC2 downregulation in mouse dorsal hippocampus was sufficient to impair memory and explored the underlying mechanisms. Using RNA interference to partially knockdown but not fully ablate KCC2 expression in a cell-type specific manner, we observed deficits in both spatial and contextual memory upon KCC2 downregulation in hippocampal principal neurons but not GABAergic interneurons. Our data indicate this effect is associated with altered hippocampal rhythmogenesis and involves, at least in part, neuronal hyperexcitability and bursting behavior.

[1]Inserm UMR-S 1270, 75005 Paris, France. [2]Sorbonne Université, 75005 Paris, France. [3]Institut du Fer à Moulin, 75005 Paris, France. [4]Neuroscience Paris Seine-Institut de Biologie Paris Seine (NPS-IBPS), 75005 Paris, France. [5]Present address: Basic Neuroscience Department, Centre Medical Universitaire, 1211 Geneva, Switzerland. ✉email: jean-christophe.poncer@inserm.fr

MATERIALS AND METHODS

RNA interference and viral vectors

In order to suppress KCC2 expression in mice, we used RNA interference with a previously validated short hairpin RNA (shRNA) sequence (shKCC2: AGCGTGTGACAATGAGGAGAACTTCCTGTCATTCTCCTCATTGTCACACGCT [37],). A sequence devoid of target in mouse genome (shNT: GGAATCTC ATTCGATGCATACCTTCCTGTCAGTATGCATCGAATGAGATTCC [28],) was used as control. These sequences were inserted in pAAV vectors under U6, CaMKII or mDlx promoters. Since the two later are polymerase II promoters, shRNA sequences were then embedded into micro-RNA (mir30) backbone [38]. Finally, once plasmids were cloned (pAAV-U6-shKCC2(shNT)-CMV-GFP-SV40, pAAV-CamKII-shmirKCC2(shmirNT)-SV40-CMV-GFP-SV40, pAAV-mDlx-GFP-shmirKCC2(shmirNT)-WPRE-SV40), they were used to produce purified AAV particles for co-expression with GFP (AAV2.1, titer 10^{13} TU/ml, Atlantic Gene Therapy, Nantes). For KCC2 expression rescue, a Flag-tagged recombinant KCC2 sequence [39] was modified to make it shRNA-proof. Mutated shRNA target sequence was synthetized (Genscript) and then subcloned in place of the original target sequence using classical digestion, ligation, and transformation. Sequence was mutated in order to prevent shRNA complementarity without changing amino-acid sequence (AACGAGGTCATCGTGAATAAATCC modified to AATGAAGTGATTGTCAACAAGTCC). The sequence was cloned into a pAAV-CamKII-KCC2flag-WPRE-SV40vector to replace the KCC2flag sequence and used to produce purified AAV particles as above.

Animals

C57BL/6JRj mice were housed in standard laboratory cages on a 12-hours light/dark cycle, in a temperature-controlled room (21 °C) with free access to food and water. Mice were purchased from Janvier Labs (Le Genest-Saint-Isle, France) and were delivered to our animal facility at least a week before surgery or behavioral testing. All procedures conformed to the International Guidelines on the ethical use of animals, the French Agriculture and Forestry Ministry guidelines for handling animals (decree 87849, license A 75-05-22) and were approved by the Charles Darwin ethical committee (agreement 2016042916319074v5).

Stereotaxic surgery

Eight-weeks old mice were anesthetized with ketamine/xylazine (100/15 mg/kg) and placed on a heating pad at 36-37 °C for the entire surgery. Ten minutes before opening the skin, lidocaine (2%) was applied locally on the skin. The virus was bilaterally injected in dorsal hippocampus (500 nl in both the dentate gyrus and CA1 for each hemisphere) at the following stereotaxic coordinates from Bregma: −1.8 mm anteroposterior (AP), ±1.2 mm mediolateral (ML) and −2.1, −2.0, −1.9, −1.3, and −1.25 mm dorsoventral (DV). This procedure usually resulted in widespread infection of the entire dorsal hippocampus. After surgery, body temperature was maintained using a heating pad under the cage until the animal recovered from anesthesia. The analgesic carprofen (0.5 mg/mouse/day) was then added to the drinking water for the next 24 hours. Behavioral experiments or electrophysiological recordings were then conducted 10 to 14 days after surgery. The spread of viral infection was systematically verified at the end of all experiments when animals were sacrificed. Only data from mice with generalized GFP expression throughout the dorsal hippocampus were considered for behavioral, biochemical or electrophysiological analysis.

Silicon probe implantation

One week after viral injection, mice were implanted with a 32 or 16-channel linear silicon probe (Neuronexus A1x32-6mm-50-177-CM32 or A1x16-5mm-50-413-CM16LP in some experiments, with 50-micron inter-electrode spacing). Mice were anesthetized with isoflurane (4% for induction, 1–2% for maintenance) in a stereotaxic frame for the entire surgery and their body temperature was maintained with a heating pad. In order to reduce pain, mice were injected with buprenorphine before surgery (0.1 mg/kg). First, the skull was cleaned and the craniotomy at the probe location was re-opened. Two screws were implanted on the frontal bone (1 per hemisphere), 1 on the parietal bone (contralateral to the probe) and 1 reference screw above the cerebellum. Then, the probe was descended into the dorsal right hippocampus at the following coordinates from Bregma: −1.8 mm (AP), −1.2 mm (ML), −2.4 mm (DV, for the 32-channels silicon probes) or −2.0 mm (DV, for the 16-channels silicon probes). Once the probe was positioned, the craniotomy was covered with Vaseline to protect the probe.

The head-stage was then built using a thin layer of SuperBond dental cement applied onto the skull, followed with Unifast TRAD dental cement on the probe and the screws. Pieces of copper mesh were then arranged around the probe to create a Faraday cage and cemented onto the skull after soldering the ground and reference of the probe with the reference electrode above the cerebellum to the copper mesh.

After surgery, body temperature was maintained with a heating pad under the cage until the animal recovered from anesthesia. The mice were then individually housed to avoid damage to the probe. For 3 days after surgery, mice were fed with high-calorie liquid chocolate and received two daily injections of buprenorphine (0.1 mg/kg s.c.). Behavioral experiments and recordings were performed one week after surgery, once the animals had fully recovered.

Canula implantation and terbinafine treatment

A home-made canula [40] was implanted into the left ventricle at the following coordinates from Bregma: −0.4 mm (AP), −1.0 mm (ML), −3.0 mm (DV), either on the day of silicon probe implantation or the day of viral injection. Mice were handled daily for a week and received 10 µL of saline injection to habituate them to intracerebroventricular (icv) injection. On the fear conditioning day, mice received 10 µL of 1 mM terbinafine solution in saline or 10 µL of saline, 30 min before experiencing the tone-shock association. They received a second injection 4 hours later. On the next day, mice received a third injection 30 minutes before testing contextual memory retrieval.

In vivo recordings and signal analysis

Animals implanted with silicon probes were connected to a recording controller (Intan Technologies, Los Angeles, USA). For sleep recordings, after a 10-minute exploration of the arena, mice were placed in their home cage. The experimenter observed the mouse and the recorded signal at all times and recorded the states of alertness: mice were considered to be sleeping when they were motionless and in a sleeping position. Sleep was further subdivided into slow-wave sleep (SWS, i.e., when slow-waves/SWR were detected in the LFP recordings) and REM (characterized by high theta activity). Mouse movements indicated wakefulness. Analyses were performed on 30 minutes of good quality SWS that were obtained, on average, during the 2 to 4 hours after exploration.

Data were acquired at 20 kHz using Intan Recording Controller software (version 2.05). All analyses were performed offline using MATLAB built-in functions, Chronux [41], the FMAToolbox (http://fmatoolbox.sourceforge.net/), as well as custom-written scripts available upon request.

Electrode positioning was assessed from layer-specific features, including spikes and ripples (in *st. pyramidale*), sharp waves (in *st. radiatum* and *st. lacunosum/moleculare*), and maximum theta power (in *st. lacunosum/moleculare*), as described in [42]. The position of the other electrodes was inferred based on the electrode spacing (50 µm) and verified *post hoc* after sacrificing the animals. Power spectra and spectrograms were computed using multi-tapers estimates on the raw LFP signal. Gamma-band was defined as 25–90 Hz. Slow and fast gamma ranges (respectively 25–55 and 60–90 Hz) were determined according to [43]. Theta power was determined in the 5–10 Hz band. Spike detection was performed using high-pass (>500 Hz) filtering and semi-automatic thresholding. Bursts of spikes were defined as a minimum of 3 spikes with inter-spike interval less than 20 ms. This value was determined from the distribution of all inter-spikes intervals (ISI) where 40–50% recordings show ISI <20 ms in our data set. Burst detection using an alternative Poisson surprise method [44] resulted in no significant difference in mean burst duration or mean number of spikes per bursts (Mann-Whitney test, $p = 0.19$ and 0.73, respectively). Ripple detection was performed by band-pass filtering (100–600 Hz), squaring and normalizing, followed by thresholding of LFP recorded in CA1 pyramidal layer. SWR were then detected semi-automatically as events exceeding a signal to noise ratio, which was manually set and varied between animals. Accurate detection of SWR was later visually confirmed on raw LFP signals.

Behavioral tests

Open field. Mice were gently placed facing the wall of a large white arena cleaned with 10% ethanol (50 × 50 × 40 cm, 90–100 lux) for a 10 minutes recording period. Their activity was recorded and analyzed using Ethovision software (Noldus). Mice were considered in the center of the arena (1/9 of the arena) when their body center was in the central zone.

Elevated-O-maze. The apparatus consisted in a white circular maze (35 cm of diameter, lane is 6 cm wide), elevated 50 cm above the floor, and divided in 4 quadrants: two opposite "closed" quadrants surrounded by 12 cm high opaque walls (the safe environment) and two "open" quadrants. The luminosity was set at 8–10 lux in the open arms and the elevated-O-maze was cleaned with 10% ethanol. Mice were placed randomly in one of the closed arms, facing an open arm. Their activity was recorded for 10 minutes and analyzed using the Ethovision software. Mice were considered in the open arms when the four paws were placed in the arm. While locomotion (average speed and distance) was estimated from the open field test, anxiety was assessed using both the open field (time spent in center) and O-maze (time spent in open arms) paradigms in order to strengthen our conclusions.

Place recognition. The arena and the objects were cleaned with 10% ethanol and the luminosity in the center of the arena was set to 10 lux in order to promote exploration. A cue card was placed on one wall to allow to orient the mice in the arena. On the three first days, mice were habituated to the arena, with two habituations per day, at least 3 hours apart. On the first habituation (H1), all mice from a single cage were placed in the arena for 30 min, allowing them to explore together the environment to help reduce stress. For the next four habituations (H2 to H5), mice were placed alone in the arena for 10 min. On the last habituation (H6), two identical objects were introduced to help reduce stress associated with novelty.

During the first exposure, 24 to 72 hours after H6, two identical objects were presented to the mouse for 10 min. Then, 10 minutes (short-term memory) or 24 hours later (long-term memory), mice were placed back in the arena with one object moved and the other in the same position. Mouse behavior was video-recorded and analyzed manually during the exposure session, in order to ensure that mice were exploring enough and did not have an initial preference for one of the objects. The data recorded during the memory test were manually scored. Exploration was considered when the mouse's head was turned toward the object and its nose was within 2 cm of the object. All manual scorings were performed blind to the experimental condition. Scoring was performed for each object sequentially on the same day, with random order between scoring sessions. A discrimination index (DI) was used as a measure of discrimination between novel and old location and obtained by dividing the difference in time spent in the old versus new locations by the total exploration time. Exploration was considered only when the animal was both in contact and facing the object.

Fear conditioning. On day 1, mice were exposed to the experimental chamber and let free to explore. Each mouse was placed four minutes in box 1 (27 x 27 cm, black environment, white light), cleaned with 70% ethanol. On the second day, mice were allowed to explore box 1 for 4 min before a tone was delivered for 30 s (4 Hz, 85 dB) that co-terminated with a two-seconds foot shock (0.25 mA) delivered through the floor grid. After a 30-second interval, the tone-foot shock procedure was repeated 3 more times. On the third day, mice were placed back in box 1 to evaluate contextual memory (i.e., without receiving any foot-shock). Freezing was then assessed during the first 3 minutes of exploration. Two hours later, they were placed in a box 2 to test cued memory. Box 2 was white and round, with no grid on the floor, red light, and was cleaned with 1% acetic acid. After 4 minutes of exploration, the tone (4 Hz, 85 dB) was played for 30 s, followed by 30 s of silence. This sequence was repeated 6 times. The freezing behavior was plotted at 30-second intervals to account for this alternating condition. The fear memory test was generally preferred to place recognition because the cue memory part of the test provides an internal, hippocampal-independent control.

The freezing behavior was analyzed manually, as described in [45, 46], blind to the experimental condition. Briefly, the experimenter watched the video for 1 second every 5 seconds and noted whether the animal was moving or freezing (no movement, mouse looking ahead). The percentage of time the animal spent freezing was then averaged. We compared our manual scoring results with those obtained with the motility detection tool of the Packwin software (v2.0.05, Panlab), with a sampling rate of 50 Hz and duration filter of 500 ms. We found that the results were similar but that manual scoring better differentiated freezing-related immobility from light activity including head movements.

Western blot analysis
Ten to fourteen days post-infection, animals were sacrificed and their brain dissected. Parasagittal slices (300–400 µm) were prepared and the infected (GFP positive) dorsal hippocampus areas were dissected under an epifluorescence macroscope. Dissected tissues were homogenized using a 2-ml Dounce homogenizer in a buffer containing 0.32 M sucrose, 2 mM HEPES, pH 7.4, 1 tablet of cOmplete™ EDTA-free protease inhibitor (Roche), 30 mM NaF, and 5 mM sodium orthovanadate. The homogenates were then centrifuged at 20,000 g for 10 min at 4 °C and the pellets resuspended in 50 mM Tris-HCl, pH 7.4. The protein concentration of all samples was then determined using a Pierce™ BCA Protein Assay Kit (Thermo Fisher). Equal amounts of proteins were then separated on a 4%–12% SDS polyacrylamide gradient gel (Invitrogen) and transferred onto a nitrocellulose membrane (GE Healthcare) at 100 V for 1 hour in order to ensure efficient transfer of high molecular weight proteins using a liquid transfer system (Bio-Rad). The membrane was blocked for one hour at room temperature in 5% milk (diluted in 1X TBS–0,1% Tween 20) then washed three times for 5 min in 1X TBS – 0,1% Tween 20. These washing conditions were used after incubation with primary and incubation with secondary steps. The membrane was incubated overnight at 4 °C with the primary antibody (diluted in 5% milk, 1X TBS – 0,1% Tween 20). Then the secondary antibody (diluted in 5% milk, 1X TBS–0,1% Tween 20) was added for 1 hour at room temperature. The membrane was then probed using the Odyssey blot imaging system (LI-COR).

The primary antibodies used were: rabbit anti-KCC2 (1:1000, Millipore), mouse anti-Tuj1 (1:10000, R&D systems), mouse anti-Flag (1:1000, M2 clone, Sigma-Aldrich) and mouse anti-GFP (1:1000, Chemicon). The secondary antibodies used were: goat anti-rabbit 800 (1:5000, Tebu-Bio or 1:15000, LiCor), goat anti-mouse 700 (1:5000, Tebu-Bio or 1:15000, LiCor).

Histology
Mice were deeply sedated using sodium pentobarbital (200 mg/kg i.p.) and then transcardially perfused with ice-cold phosphate buffer saline (PBS) solution, followed by ice-cold 4% paraformaldehyde (PFA) in PBS pH 7.4. Extracted brains were fixed in 4% PFA overnight and then equilibrated in 30% sucrose in PBS. A sliding cryotome was used to section the brains into 40 µm-thick coronal sections. Immunohistochemistry experiment was performed when necessary. Only mice with a minimal infection spread of 500 µm in both dorsal hippocampi (CA1, CA3, DG) were considered for further behavioral analysis.

Immunohistochemistry
Slices were incubated for 1 hour at room temperature in a blocking solution containing 10% goat serum, 0.1% Triton X-100 in PBS. Incubation with primary antibody (rabbit anti-KCC2 (1:500, Millipore), chicken anti-GFP (1:1000, Millipore), mouse anti-Flag (1:1000, Sigma-Aldrich), mouse anti-GAD67 (1:1000, Abcam)) was then performed in blocking buffer overnight at 4 °C. After 3 × 10 min washes in PBS, slices were incubated with secondary antibodies with a dilution of 1:1000 in blocking buffer for 1 hour (goat anti-rabbit-cy3, donkey anti-mouse-cy5, donkey anti-chicken-488 (Jackson Labs)). After another 3 × 10 min washes, slices were mounted on a coverslip in Mowiol/Dabco (25 mg/mL) solution. Immunofluorescence images were acquired using an upright confocal microscope (Leica TCS SP5), using a 40X 1.30-N.A. objective and Ar/Kr laser set at at 491 and 561 nm for excitation of Cy3 and FITC, respectively, for images of the entire hippocampus. Stacks of 25–30 µm optical sections were acquired at 512 x 512 pixel resolution with a z-step of 1 µm.

Statistics
All statistical tests were performed using SigmaPlot 13 software (Systat Software Inc.). When necessary, proportions were arcsin-transformed prior to performing appropriate statistical test. Comparison of means was performed using Student's t-test for normally distributed variables (as tested with Shapiro-Wilk test) of equal variances (Brown-Forsythe test). t-values and degrees of freedom (DF) are indicated in figure legends. Otherwise, comparison of mean was performed using the non-parametric Mann-Whitney rank sum test. Two-way ANOVA was used for comparison of distributions when data were normally distributed with equal variances. Kolmogorov-Smirnov test was used to compare distributions. Statistical significance was set to $p \leq 0.05$.

RESULTS
KCC2 down-regulation in dorsal hippocampal neurons impairs spatial and contextual memory in mice
Genetic ablation of *Slc12a5* encoding the KCC2 transporter in mice is associated with severe developmental defects leading to
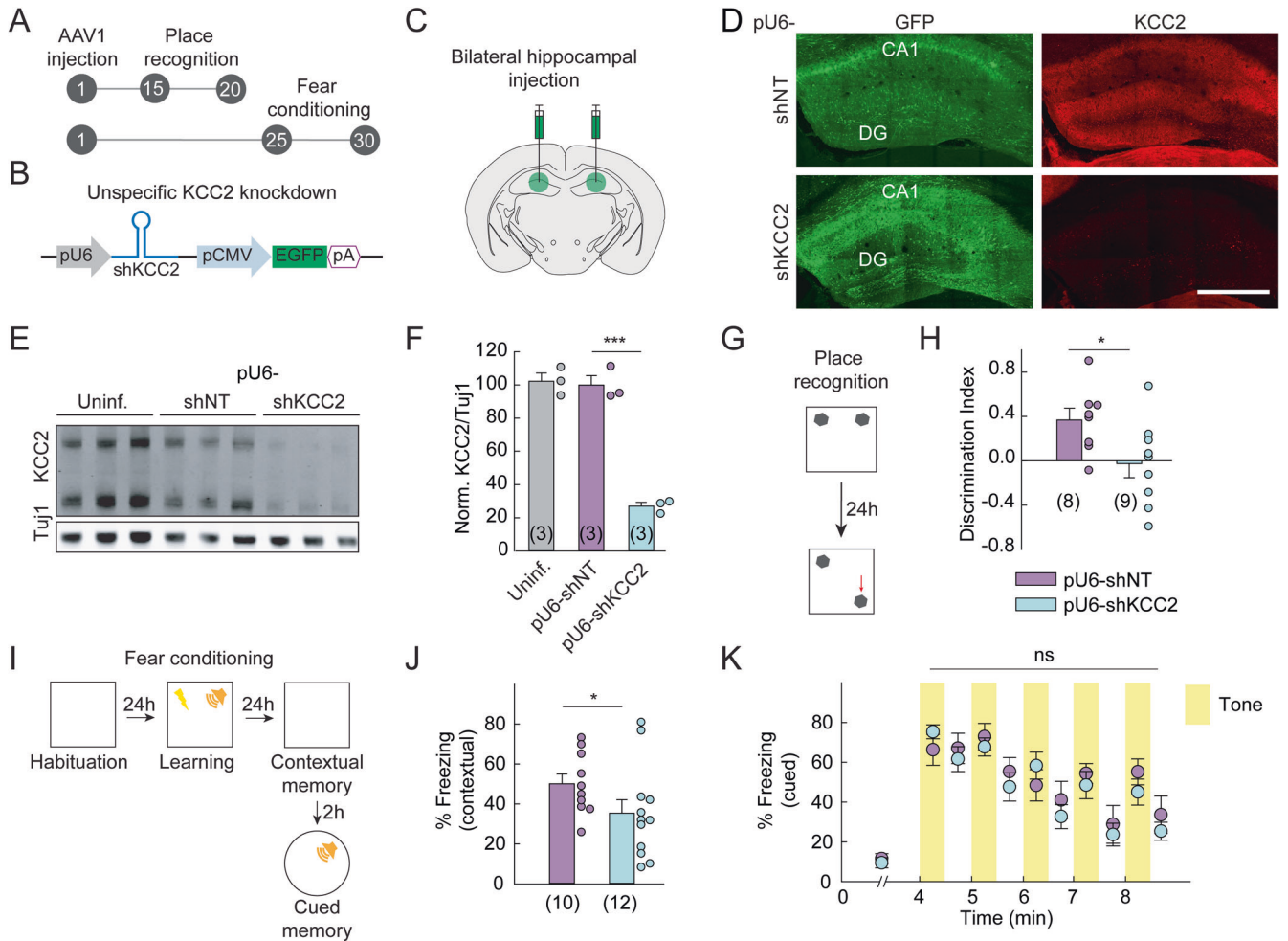
Fig. 1 KCC2 down-regulation in dorsal hippocampus impairs spatial and contextual memory. A Timeline of the experiment (days). **B** Design of the viral vector for unspecific KCC2 knockdown. **C** Wild-type mice were injected bilaterally in the dorsal hippocampus with AAV vector designed to knockdown KCC2. **D** Representative confocal maximal projection images of hippocampal coronal sections immunostained for GFP and KCC2 from mice infected with U6-shNT or U6-shKCC2-expressing AAV vectors, showing massive KCC2 knockdown throughout hippocampal fields in the later. Scale: 500 μm. **E** Representative immunoblot of KCC2 in hippocampal protein extracts from non-infected mice ($n = 3$) and mice infected either with U6-shNT ($n = 3$) or U6-shKCC2 ($n = 3$) expressing viruses. **F** Quantification of KCC2 expression, relative to that from mice infected with U6-shNT vector (t-test, $t = 11.9$, DF = 4, $p < 0.001$). Tubulin was used as an internal standard. **G** Protocol of the place recognition task. **H** Impaired spatial memory is observed in KCC2-knockdown mice compared to controls with a higher discrimination index. (t-test, $t = 2.3$, DF = 15, $p = 0.017$). **I** Protocol of the fear conditioning task. **J** In the contextual memory test, freezing was assessed during the first 3 minutes of exploration of the foot-shock associated cage. Mice infected with U6-shKCC2 vector display reduced freezing time compared to mice infected with U6-shNT vector (t-test, $t=1.7$, DF = 20, $p = 0.050$). **K** Summary graph showing the time course of freezing upon exposure to foot-shock associated sound. Cued memory retention shows no difference between both groups.

premature death around birth, due to respiratory complications [47] and seizures [48]. In order to evaluate the impact of KCC2 downregulation, as observed in the human pathology, independent of developmental defects associated with constitutive ablation, we used virus-based chronic silencing by RNA interference. Adult mice were infected bilaterally in dorsal hippocampus with AAV vectors expressing either non-target (shNT) or previously validated KCC2-specific (shKCC2) shRNAs [37] (Fig. 1A–C). Effective KCC2 downregulation was verified after 2–4 weeks by immunostaining (Fig. 1D) and western blot analysis of micro-dissected hippocampal extracts (Fig. 1E, F). KCC2 expression was reduced by >70% in hippocampal extracts from mice infected with virus expressing shKCC2 as compared to shNT (t-test $p < 0.001$). Viral infection per se resulted in no change in KCC2 expression, with no significant difference between samples from mice infected with control (shNT) virus and non-infected animals (t-test $p = 0.388$).

We next explored the effects of chronic KCC2 downregulation on mouse behavior. No consistent difference was observed between control and KCC2 knockdown mice in terms of locomotor activity or anxiety (Supplementary Fig. S1). Thus, we tested whether KCC2 downregulation might affect hippocampus-dependent spatial [49, 50] and contextual memory. In an object-place recognition paradigm (Fig. 1G), mice explored two identical objects for 10 minutes in an arena with a cue card, and one of the objects was moved to a new location in the arena 24 hours later. While control mice showed a significant preference for the moved object (Fig. 1H), this preference was significantly reduced in KCC2-knockdown mice (t-test $p = 0.017$). This shows that KCC2 silencing in dorsal hippocampus compromises spatial memory. We next evaluated the performance of mice in contextual and cued fear memory. Mice received 4 foot-shocks associated with a tone on the training day. On the next day, contextual and cued memories were tested (Fig. 1I). In the hippocampus-dependent contextual
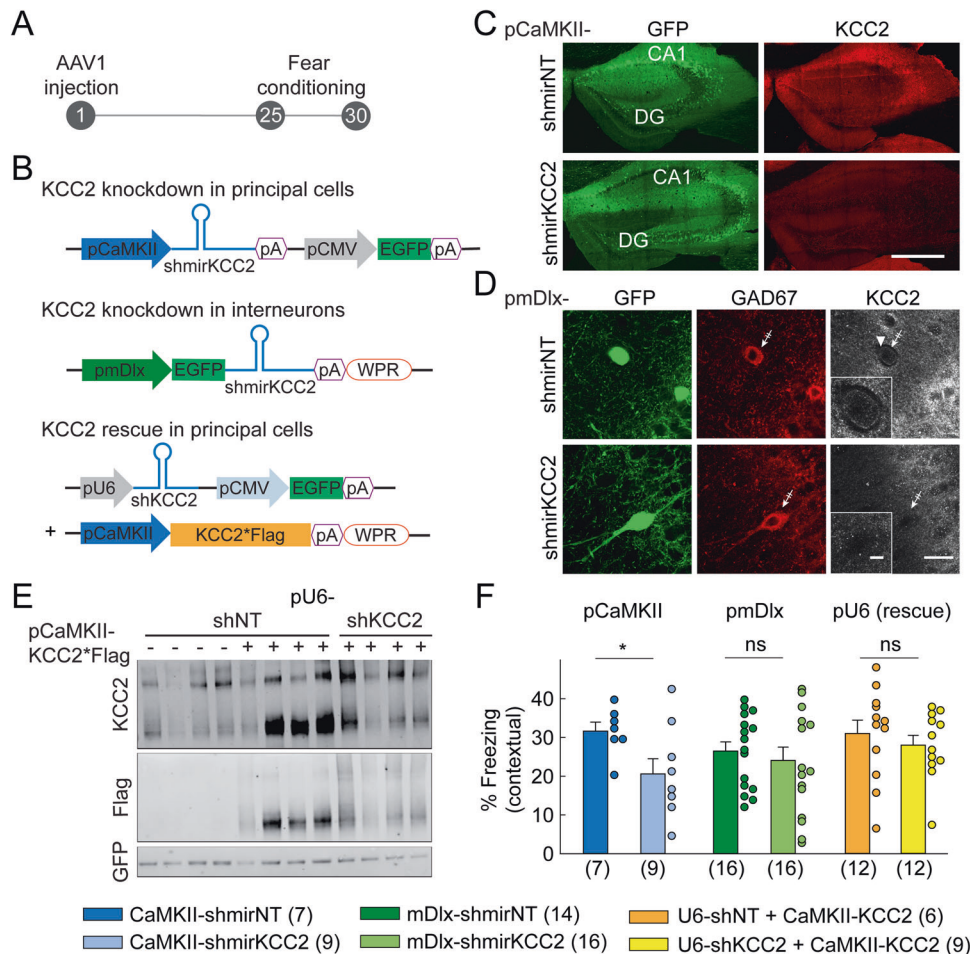
Fig. 2 KCC2 down-regulation in principal cells is sufficient to alter contextual memory. A Timeline of the experiment (days). **B** Viral vectors used to knockdown KCC2 in principal cells or interneurons, or to rescue KCC2 expression in principal cells. KCC2*Flag indicates shRNA-proof, Flag-tagged KCC2 sequence. **C** Representative confocal maximal projection images of hippocampal coronal sections immunostained for GFP and KCC2 from mice infected with CaMKII-shNT or CaMKII-shKCC2-expressing vectors, showing massive KCC2 knockdown in the later. Scale: 500 μm. **D** Representative confocal maximal projection images of area CA1 of hippocampal coronal sections immunostained for GFP, GAD67, and KCC2 from mice infected with vectors expressing mDlx-shmirNT or mDlx-shmirKCC2. Arrowheads show infected cells are GAD67+ interneurons and that mDlx-shmirKCC2 efficiently suppressed KCC2 expression in these cells, as evidenced by lack of somatic KCC2 immunostaining (crossed out arrows). Scale: 20 μm. **E** Representative immunoblot of KCC2, GFP, and Flag in hippocampal protein extracts from mice infected with U6-shNT or U6-shKCC2 and CamKII-KCC2*Flag expressing vectors showing CamKII-KCC2*Flag efficiently restored KCC2 expression upon knockdown. **F** Summary graph for contextual memory, showing the percent time spent freezing during the first 3 minutes of exploration of the foot-shock associated cage in a fear conditioning paradigm, revealing reduced freezing in mice infected with CaMKII-shmirKCC2 expressing vector as compared with mice infected with CaMKII-shmirNT vector (t-test, $t = 2.3$, $DF = 14$, $*p = 0.019$ for CaMKII-shmirKCC2). Mice infected with mDlx-shmirKCC2 vector or with U6-shKCC2 and CamKII-KCC2*Flag show no alteration of freezing behavior as compared to control mice.

memory test, the freezing response of KCC2-knockdown (shKCC2) mice was significantly reduced compared to that of control (shNT) mice (Fig. 1J; t-test $p = 0.050$). However, no difference in freezing behavior was observed between the two groups in the sound-cued memory test (Fig. 1K; two-way repeated measures ANOVA $p = 0.329$), which primarily depends on the amygdala and not the hippocampus [51]. Our results therefore suggest that chronic KCC2 downregulation in the dorsal hippocampus specifically impairs both spatial and contextual memory.

KCC2 silencing in hippocampal principal neurons is sufficient to compromise contextual memory
We next aimed to explore the cellular and network mechanisms underlying memory deficits upon KCC2 knockdown in dorsal hippocampus. Since KCC2 is expressed in both hippocampal principal cells and at least some interneuron subtypes [52, 53], we tested whether KCC2 silencing in either neuron subtype might be

sufficient to recapitulate memory deficits induced by unspecific silencing. In order to specifically suppress KCC2 expression in principal neurons or interneurons, shRNA sequences were imbedded into a mir30 backbone [38] and inserted downstream Pol II promoters specific to either cell type in the forebrain (pCamKII [54] and pmDlx [55], respectively) (Fig. 2B). These constructs efficiently suppressed KCC2 expression in principal neurons and interneurons of dorsal hippocampus, respectively, as illustrated by immunofluorescence detection (Fig. 2C, D). Five to six weeks following viral injection, mice were then exposed to a fear-conditioning paradigm (Fig. 2A). During the contextual memory test, mice infected with a virus expressing pCaMKII-shmirKCC2 targeting principal neurons showed significantly less freezing than control mice (t-test $p = 0.019$; Fig. 2F), comparable to the effect observed in mice with cell-type unspecific silencing (Fig. 1J). In contrast, mice infected with a virus expressing pmDlx-shmirKCC2 targeting GABAergic interneurons displayed a freezing

response comparable to that of the control group (t-test $p = 0.215$). Again, mice expressing either pCaMKII-shmirKCC2 or pmDlx-shmirKCC2 in the dorsal hippocampus showed no deficit in cued memory as compared to their respective controls (Supplementary Figure S2).

These results show that KCC2 silencing only in the dorsal hippocampal principal neurons, but not interneurons, is sufficient to impair contextual fear memory. In order to further test the specificity of our knockdown approach, we then performed a rescue experiment in which KCC2 silencing was induced in dorsal hippocampus using an AAV1-pU6-shKCC2-CMV-GFP vector and then specifically rescued in principal cells using an AAV1-pCaMKII-KCC2*Flag vector, expressing a Flag-tagged and shRNA-proof recombinant KCC2 (Fig. 2B). Co-infection was confirmed by western blot analysis with GFP and Flag antibodies (Fig. 2E). In animals co-expressing pU6-shKCC2 and pCamKII-KCC2Flag, total KCC2 expression increased almost 2-fold (1.93 ± 0.59, $n = 4$), compared to control animals infected with virus expressing only pU6-shNT. For comparison, co-infection with viruses expressing pU6-shNT and pCamKII-KCC2Flag resulted in a 3-fold increase in KCC2 expression (3.27 ± 0.91, $n = 4$) compared with controls. These data show that co-expression of pCamKII-KCC2Flag very effectively restores KCC2 expression in knockdown animals.

Recombinant KCC2 overexpression only in principal cells fully restored contextual memory in mice with cell-type unspecific KCC2 silencing (Mann-Whitney test, $p = 0.402$; Fig. 2F). Again, none of these manipulations induced significant change in anxiety (Fig. S1B–D) or locomotor activity (Fig. S1–F), as evaluated in open field and elevated-O-maze tests. These data show that KCC2 knockdown in principal neurons recapitulates the behavioral impact of unspecific neuronal knockdown. Since no evidence supports a cell-type specific KCC2 downregulation in the pathology, the remaining of our analysis was performed using the non-specific pU6 construct.

KCC2 silencing enhances neuronal excitability and impairs hippocampal rhythmogenesis

Memory consolidation relies in part on hippocampal rhythmic activities [36], such as theta- and gamma-band activities that occur during rapid eye movement (REM) sleep [56, 57], as well as sharp-wave ripples (SWRs) associated with non-REM sleep and immobility [33, 58]. Such activities involve temporally precise interactions between glutamatergic and GABAergic neurons [59–63]. Since KCC2 knockdown is known to affect both glutamatergic [27, 28] and GABAergic [2, 32, 64] synaptic function as well as neuronal excitability [32], we hypothesized that these combined effects may impair hippocampal rhythmogenesis. To test this hypothesis, we bilaterally injected mice with AAV1-pU6-shNT or AAV1-pU6-shKCC2 vectors in the dorsal hippocampus and then implanted a silicon probe in one hippocampus (Fig. 3A–C). The silicon probe was positioned to record LFP signal throughout the CA1 to DG axis.

Theta-band activity (5–10 Hz) was recorded throughout hippocampal layers during REM sleep, with maximal power within *st. lacunosum/moleculare*, as previously reported [32, 57] (Fig. 3D–E). No difference was observed in the power profile of theta-band activity between KCC2 knockdown and control mice (Kruskal-Wallis test $p = 0.774$). Gamma-band activity is also detected during various behavioral states including REM sleep and can be divided in slow (25–55 Hz) and fast (60–90 Hz) gamma components, with distinct underlying mechanisms and functional impact on memory encoding and consolidation [36, 60]. We, therefore, distinguished the two components and observed a significant and specific decrease in the power of slow (Kruskal-Wallis test $p = 0.003$, Fig. 3E) but not fast gamma oscillations ($p = 0.247$) in KCC2 knockdown mice as compared to control.

We then tested whether KCC2 silencing might affect SWRs during slow-wave sleep (Fig. 3F–H). Whereas SWR duration increased modestly (by about 10%) in KCC2 knockdown as compared to control mice, their mean rate increased by 140% (Fig. 3H; Kolmogorov-Smirnov test $p < 0.001$ for both). However, their time-frequency profiles were similar, with no sign of high-frequency oscillation or fast-ripple component (250–500 Hz) that represent hallmarks of the epileptic hippocampus [65, 66] (Fig. 3G). This lack of epileptiform activity was consistent with the lack of spontaneous seizures in KCC2 knockdown animals observed during weeks of behavioral evaluation.

More strikingly, however, we observed a large and significant increase (by about 125 % on average) in multiunit activity (MUA) within *st. pyramidale* of CA1 of KCC2 knockdown mice as compared to controls (Fig. 3F, I). This increase in frequency (Kolmogorov-Smirnov test $p < 0.001$, Fig. 3I) was not homogenous but was associated with a remarkable (+268%) increase in the occurrence of bursts of MUA (Kolmogorov-Smirnov test $p < 0.001$; Fig. 3F, I). This increased burst frequency was not just a mere reflection of the increased MUA, as the burst event fraction (number of bursts divided by the number of spike trains) was also significantly increased in KCC2 knockdown mice (Fig. 3J; Mann-Whitney test, $p = 0.010$). Moreover, spike bursts were more often associated with ripples than in control mice (Fig. 3J, Mann-Whitney test, $p = 0.010$).

Altogether, these results show that KCC2 downregulation in dorsal hippocampus affects hippocampal rhythmogenesis by (i) reducing slow gamma rhythm during REM sleep, (ii) increasing SWR rate and duration and (iii) increasing MUA and bursting in CA1 as well as promoting spike bursts during SWRs. Such neuronal hyperexcitability may then generate unspecific *noise* and compromise memory consolidation [67], thereby contributing to impaired hippocampus-dependent memory.

The specific Task-3 channel opener terbinafine reduces neuronal excitability and occludes memory impairment upon KCC2 silencing

KCC2 interaction with leak potassium channel Task-3 controls membrane trafficking and expression of Task-3, thereby influencing membrane resistance and excitability [32]. Thus, reducing KCC2 expression was shown to increase hippocampal principal neuron excitability in vitro, independently of changes in GABAergic signaling. This effect promoted anomalous recruitment of dentate granule cells during dentate spikes which was prevented by chemogenetic silencing of granule cells in vivo [32]. We hypothesized a similar effect may also contribute to increase neuronal firing and contamination of SWRs with bursts of action potentials upon KCC2 knockdown. We therefore tested whether increasing Task-3 function, using the selective activator terbinafine [68, 69], might prevent neuronal hyperexcitability and thereby rescue or occlude memory upon KCC2 silencing. In KCC2-knockdown mice, we implanted an intracerebroventricular (icv) canula and a silicon probe to record neuronal activity in the right dorsal hippocampus while injecting terbinafine in the left lateral ventricle (Fig. 4A). Infusion of terbinafine (10 µl, 1 mM solution) but not saline reduced multiunit activity in the CA1 area by about 40% for up to two hours (Fig. 4C–E, t-test $p = 0.013$).

Terbinafine intraventricular infusion had no significant effect on speed, immobility time, or time spent in the center of the arena, suggesting terbinafine has no major effect on locomotion or anxiety compared to saline (Fig. S3). We then tested the effect of terbinafine infusion on contextual memory in mice following KCC2 silencing. Mice were infected with either the pU6-shKCC2 or pU6-shNT viral vector and a canula was implanted to allow infusion of terbinafine or saline as a control. As in previous experiments, KCC2-knockdown mice receiving saline infusion showed reduced freezing as compared to control mice in a contextual fear memory paradigm (t-test $p = 0.023$; Fig. 4F, G). However, in mice receiving intraventricular terbinafine infusion, no difference in freezing was observed between KCC2-knockdown
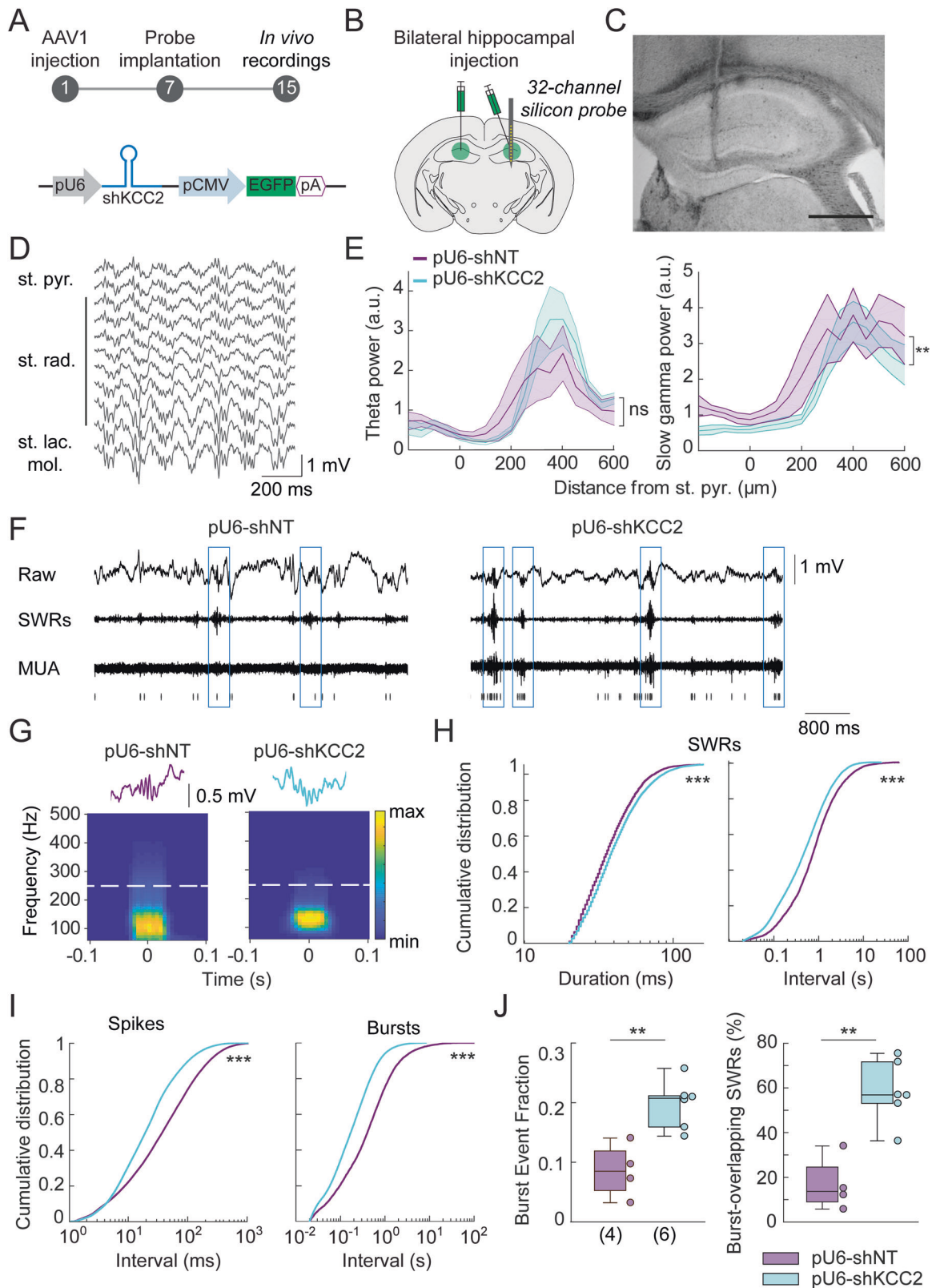
mice and controls (t-test $p = 0.104$). Noticeably, control mice receiving terbinafine infusion showed a slight reduction in freezing levels compared to saline-treated mice (t-test, $p = 0.056$), suggesting intraventricular terbinafine treatment might also partially impair contextual memory. Interestingly, however, infusion of terbinafine did not further affect contextual memory in KCC2 knockdown mice. Together, our results show that a Task-3 channel activator reduces neuronal excitability and occludes the impairment of contextual memory induced by KCC2 silencing in dorsal hippocampus.

Fig. 3 KCC2 downregulation leads to hippocampal network hyperexcitability. A Timeline of the experiment (days) and viral vector used for KCC2 knockdown. **B** Following the bilateral viral injection to knockdown KCC2 in dorsal hippocampus, a 16 or 32-channel linear silicon probe was implanted. **C** Widefield macroscope image of dorsal hippocampus near implantation site showing the track of the implanted probe through CA1 and the dentate gyrus. Scale: 500 µm. **D** Representative example of REM sleep recordings in mice infected with U6-shNT expressing vector. **E** Left, theta power in the 5–10 Hz band measured during REM sleep using multi-tapers estimates. Power (in arbitrary units, a.u.) is plotted as a function of the electrode localization with respect to *st.pyramidale*. Theta power profile was not affected upon KCC2 knockdown (Kruskal-Wallis test, $p = 0.774$). Right, slow gamma (25–55 Hz) power plotted as a function of the electrode localization with respect to *st.pyramidale*. Slow gamma power was reduced upon KCC2 knockdown (Kruskal-Wallis test, **$p = 0.003$; n = 5 control and 6 KCC2 knockdown mice). **F** Representative examples of LFP signal recorded in CA1 *st.pyramidale* in mice infected with U6-shNT or U6-shKCC2 expressing vectors during non-REM sleep. The signal was filtered to detect either sharp wave ripples (SWRs, boxed in blue, 100-300 Hz) or multiunit activity (MUA, >500 Hz), as indicated in raster plot below. **G** Top, representative recordings of individual ripples from mice infected with U6-shNT or U6-shKCC2 expressing vectors. Bottom, time-frequency plots showing the average frequency over time of all ripples in recordings from 4 control and 5 KCC2 knockdown mice. Note the lack of high-frequency oscillations or fast ripples (>250 Hz) in either condition. **H** Cumulative distribution functions of ripple duration (left) and inter ripple interval (right). Upon KCC2 knockdown, both ripple duration and frequency significantly increased (Kolmogorov–Smirnov test, ***$p < 0.001$). **I** Cumulative distribution functions of inter-spike (left) and inter-burst (right) intervals. MUA frequency as well as burst frequency were increased in KCC2-knockdown mice compared to controls (Kolmogorov–Smirnov test, ***$p < 0.001$; n = 4 control and 6 KCC2 knockdown mice). **J** Summary boxplots showing the distribution of burst event fraction (number of bursts relative to the number of spike trains) (left) and proportion of ripples associated with bursts of MUA activity (right). Both were significantly increased upon KCC2 knockdown (Mann-Whitney test, **$p = 0.010$; n = 4 control and 6 KCC2 knockdown mice).
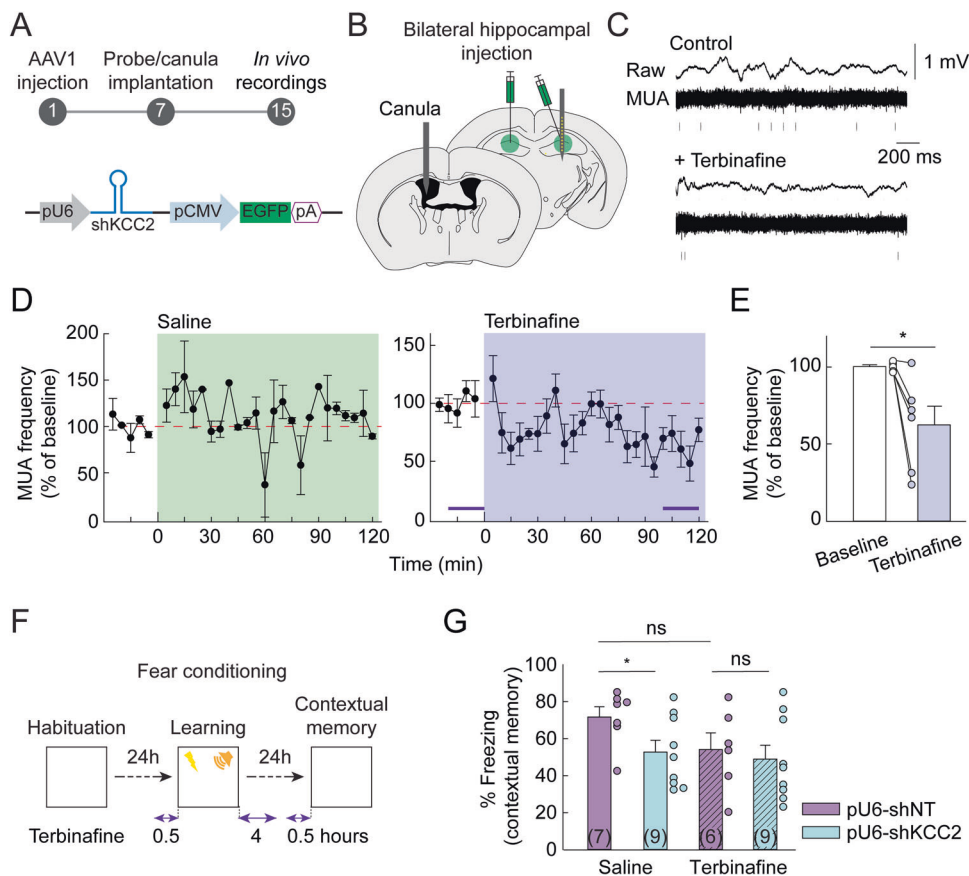

Fig. 4 Task-3 channel activator terbinafine occludes memory deficits upon KCC2 knockdown. A Experimental timeline (days) and viral vector used in these experiments. **B** A week after bilateral hippocampal injection of AAVs to knockdown KCC2, a silicon probe and a cannula were implanted in the right hippocampus and left lateral ventricle, respectively. **C** Representative examples of LFP signals recorded in CA1 *st.pyramidale* of mice infected with U6-shKCC2 expressing vectors, before and after icv injection of terbinafine (10 µL of 1 mM solution). The signal was filtered to detect multiunit activity (MUA, >500 Hz). **D** Summary plots showing MUA frequency over time, normalized to control (prior to icv injection) in animals infected with U6-shKCC2 vector, with saline (left, $n = 4$ from 2 mice) or terbinafine (right, $n = 6$ from 2 mice). **E** Summary graph showing MUA frequency before and 110 min following icv terbinafine injection. (t-test, $t = 2.6$, DF = 10, *$p = 0.013$). **F** Timeline of the fear conditioning paradigm with icv injection of saline or terbinafine. **G** Summary plot showing % time spent freezing during 3 minutes of exploration of the foot-shock associated cage. Saline-injected mice infected with U6-shKCC2 vector display reduced freezing compared to control mice infected with U6-shNT expressing vector (t-test, $t = 2.2$, DF = 14, *$p = 0.023$). However, this effect was occluded by icv infusion of terbinafine (t-test, $t = 0.4$, DF = 13, $p = 0.346$). Terbinafine induced a noticeable yet non-significant reduction of freezing in the control group (U6-shNT, t-test, $t = 1.7$, DF = 11, $p = 0.06$).

DISCUSSION

We show that chronic KCC2 downregulation in the dorsal hippocampus induces spatial and contextual memory deficits that can be mimicked by KCC2 silencing in principal neurons but not GABAergic interneurons. This memory impairment is associated with neuronal hyperexcitability and bursting as well as altered hippocampal rhythmogenesis, but no detectable spontaneous epileptiform activity. Finally, our results show that intraventricular administration of terbinafine, a specific Task-3 channel activator, reduces neuronal hyperexcitability and occludes contextual memory impairment upon KCC2 silencing in dorsal hippocampus.

Reduced neuronal KCC2 expression has been reported in animal models of epilepsy [9, 70] as well as postoperative tissue from intractable epilepsy patients [10, 11, 71–73]. Computational modeling predicted that complete KCC2 suppression in only 30% of principal neurons may be sufficient to promote seizures, at least under conditions of neuronal hyperexcitability [25]. Here, this hypothesis was tested experimentally and show that chronic reduction in KCC2 expression throughout mouse dorsal hippocampus affects neuronal and network activity but fails to trigger detectable epileptiform activity or seizures. Similarly, no sign of an epileptic network was detected upon KCC2 knockdown in rat dentate gyrus [32]. These results contrast with those obtained upon complete genetic ablation of the KCC2b isoform [74] or conditional deletion of KCC2 carboxy-terminal domain in mouse dorsal hippocampus [75], both leading to spontaneous seizures. This suggests that the complete loss of KCC2 expression or expression of a truncated, likely dysfunctional transporter induce a more severe phenotype than that induced by KCC2 downregulation as observed in the pathology. Further supporting this conclusion, hypomorphic KCC2-deficient mice retaining 15–20% of normal KCC2 expression also failed to display spontaneous seizures [76].

Our data therefore demonstrate that memory deficits are induced by KCC2 downregulation independent of epileptiform activity. Memory involves a sequence of events (encoding, consolidation and retrieval [36, 77]) which may all, in principle, be affected by KCC2 downregulation. Expression of long-term potentiation, a key mechanism for engram formation and selection [78, 79], is hindered upon KCC2 knockdown in hippocampal neurons due to altered activity-dependent AMPA receptor trafficking in dendritic spines [27]. Impaired hippocampal LTP may thus contribute to the spatial and contextual memory deficits upon KCC2 downregulation in dorsal hippocampus. In addition, hippocampal rhythmogenesis is involved in both memory encoding and consolidation [36]. Given the importance of GABA signaling in both hippocampal theta- and gamma-band oscillations [80, 81], which are critical to memory encoding and retention [36, 82], it is remarkable that KCC2 downregulation had only little effect on these oscillations, with only a moderate reduction of slow gamma band activity power. This may reflect the relative preservation of the driving force of GABAA receptor-mediated currents upon KCC2 knockdown, due to the parallel depolarization of their reversal potential and of resting membrane potential [32]. SWRs however were affected by KCC2 downregulation, with an increased frequency of occurrence but only a moderate effect on duration and no effect on their frequency components. SWR initiation is thought to be triggered by a gradual buildup of principal cell activity in the recurrent CA3 network, which in turn recruits parvalbumin interneurons to generate the major component of the ripple [83]. Therefore, the increased frequency of SWRs upon KCC2 knockdown cannot be specifically attributed to altered KCC2 function in interneurons and likely reflects a combination of changes in both neuronal excitability and GABA signaling. Of note, increasing the duration (>100 ms) but not the frequency of hippocampal SWRs has been shown to improve spatial memory performance in rats [84].

Instead, KCC2 silencing induced only a very modest (about 10%) increase in SWR duration but a 2-fold increase in their frequency. Collectively, these data suggest that the observed alterations in SWR properties may not primarily contribute to degrading memory performance upon KCC2 knockdown. Instead, we suggest coincidence with spike bursts may degrade their information content and memory consolidation.

Thus, one of the most striking alteration of hippocampal activity induced upon KCC2 knockdown was increased neuronal firing and bursting. This effect on neuronal excitability is reminiscent of that reported for the first time upon genetic ablation of KCC2 in cerebellar granule cells [85]. It was particularly apparent during non-REM sleep, where bursts of multiunit activity often superimposed with SWRs, which play a crucial role in memory consolidation [33, 58]. The identity of hyperexcitable neurons could not be resolved in this study, as our silicon probe layout with a 50 μm electrode spacing did not allow reliable spike sorting and distinction between principal cells and interneurons. During SWRs, co-firing patterns of neurons activated during previous wakefulness are replayed [86], likely contributing to memory consolidation. Neuronal hyperexcitability and bursting resulting from KCC2 knockdown may then act to scramble the information content of replay firing sequences, thereby compromising the specificity of memory consolidation. Nonspecific firing of just few hippocampal CA1 neurons was indeed shown to compromise reactivation of memory engram cells [67]. Increased hippocampal activity correlating with cognitive decline has been reported in aging rodents and can be rescued by using low doses of antiepileptic drugs acting to decrease neuronal excitability [87–89]. Similarly, here, normalizing neuronal activity with a Task3-specific channel opener occluded the contextual memory deficits induced by KCC2 suppression, suggesting neuronal hyperexcitability may play a critical role in these deficits. It is unlikely that this effect of terbinafine reflects a nonspecific disturbance in mouse behavior, because no changes in locomotion or anxiety were observed upon terbinafine infusion. Further exploration of the behavioral effects of terbinafine, however, would clarify its impact on memory performance and better predict its therapeutic potential.

Together, our results demonstrate that KCC2 downregulation, as observed in numerous neurological and psychiatric disorders, leads to neuronal hyperexcitability and memory impairment and that Task-3 channels openers, like KCC2 enhancers [19, 90], may be of therapeutic interest for cognitive deficits associated with these disorders. Further work is now needed to test this possibility. Computational modeling may help disentangle the respective contributions of altered chloride transport and neuronal hyperexcitability in the emergence of pathological activities.

REFERENCES

1. Kaila K, Price TJ, Payne JA, Puskarjov M, Voipio J. Cation-chloride cotransporters in neuronal development, plasticity and disease. Nat Rev Neurosci. 2014;15: 637–54.
2. Rivera C, Voipio J, Payne JA, Ruusuvuori E, Lahtinen H, Lamsa K, et al. The K+/Cl-co-transporter KCC2 renders GABA hyperpolarizing during neuronal maturation. Nature 1999;397:251–5.
3. Virtanen MA, Uvarov P, Mavrovic M, Poncer JC, Kaila K. The multifaceted roles of KCC2 in cortical development. Trends Neurosci. 2021;44:378–92.
4. Bonislawski DP, Schwarzbach EP, Cohen AS. Brain injury impairs dentate gyrus inhibitory efficacy. Neurobiol Dis. 2007;25:163–9.
5. Sawant-Pokam PA, Vail TJ, Metcalf CS, Maguire JL, McKean TO, McKean NO, et al. Preventing neuronal edema increases network excitability after traumatic brain injury. J Clin Investig. 2020;130:6005–20.
6. Jaenisch N, Witte OW, Frahm C. Downregulation of potassium chloride cotransporter KCC2 after transient focal cerebral ischemia. Stroke; a J Cereb Circ. 2010;41:e151–9.
7. MacKenzie G, Maguire J. Chronic stress shifts the GABA reversal potential in the hippocampus and increases seizure susceptibility. Epilepsy Res. 2015;109:13–27.

8. Sarkar J, Wakefield S, MacKenzie G, Moss SJ, Maguire J. Neurosteroidogenesis is required for the physiological response to stress: role of neurosteroid-sensitive GABAA receptors. J Neurosci: Off J Soc Neurosci. 2011;31:18198–210.

9. Pathak HR, Weissinger F, Terunuma M, Carlson GC, Hsu FC, Moss SJ, et al. Disrupted dentate granule cell chloride regulation enhances synaptic excitability during development of temporal lobe epilepsy. J Neurosci: Off J Soc Neurosci. 2007;27:14012–22.

10. Huberfeld G, Wittner L, Clemenceau S, Baulac M, Kaila K, Miles R, et al. Perturbed chloride homeostasis and GABAergic signaling in human temporal lobe epilepsy. J Neurosci: Off J Soc Neurosci. 2007;27:9866–73.

11. Pallud J, Le Van Quyen M, Bielle F, Pellegrino C, Varlet P, Labussiere M, et al. Cortical GABAergic excitation contributes to epileptic activities around human glioma. Sci Transl Med. 2014;6:244ra89.

12. Rivera C, Voipio J, Thomas-Crusells J, Li H, Emri Z, Sipila S, et al. Mechanism of activity-dependent downregulation of the neuron-specific K-Cl cotransporter KCC2. J Neurosci: Off J Soc Neurosci. 2004;24:4683–91.

13. Arion D, Lewis DA. Altered expression of regulators of the cortical chloride transporters NKCC1 and KCC2 in schizophrenia. Arch Gen Psychiatry. 2011;68:21–31.

14. Hyde TM, Lipska BK, Ali T, Mathew SV, Law AJ, Metitiri OE, et al. Expression of GABA signaling molecules KCC2, NKCC1, and GAD1 in cortical development and schizophrenia. J Neurosci: Off J Soc Neurosci. 2011;31:11088–95.

15. Sullivan CR, Funk AJ, Shan D, Haroutunian V, McCullumsmith RE. Decreased chloride channel expression in the dorsolateral prefrontal cortex in schizophrenia. PloS one. 2015;10:e0123158.

16. Bertoni A, Schaller F, Tyzio R, Gaillard S, Santini F, Xolin M, et al. Oxytocin administration in neonates shapes hippocampal circuitry and restores social behavior in a mouse model of autism. Mol Psychiatry. 2021;26:7582–95.

17. Banerjee A, Rikhye RV, Breton-Provencher V, Tang X, Li C, Li K, et al. Jointly reduced inhibition and excitation underlies circuit-wide changes in cortical processing in Rett syndrome. Proc Natl Acad Sci USA. 2016;113:E7287–96.

18. Duarte ST, Armstrong J, Roche A, Ortez C, Perez A, O'Callaghan Mdel M, et al. Abnormal expression of cerebrospinal fluid cation chloride cotransporters in patients with Rett syndrome. PloS one. 2013;8:e68851.

19. Tang X, Drotar J, Li K, Clairmont CD, Brumm AS, Sullins AJ, et al. Pharmacological enhancement of KCC2 gene expression exerts therapeutic effects on human Rett syndrome neurons and Mecp2 mutant mice. Sci Transl Med. 2019;11:eaau0164.

20. Dillon DG, Pizzagalli DA. Mechanisms of memory disruption in depression. Trends Neurosci. 2018;41:137–49.

21. Dupont S, Van de Moortele PF, Samson S, Hasboun D, Poline JB, Adam C, et al. Episodic memory in left temporal lobe epilepsy: a functional MRI study. Brain: J Neurol. 2000;123:1722–32.

22. Lim C, Alexander MP. Stroke and episodic memory disorders. Neuropsychologia 2009;47:3045–58.

23. Gur RC, Gur RE. Memory in health and in schizophrenia. Dialogues Clin Neurosci. 2013;15:399–410.

24. Kaila K, Ruusuvuori E, Seja P, Voipio J, Puskarjov M. GABA actions and ionic plasticity in epilepsy. Curr Opin Neurobiol. 2014;26:34–41.

25. Buchin A, Chizhov A, Huberfeld G, Miles R, Gutkin BS. Reduced efficacy of the KCC2 cotransporter promotes epileptic oscillations in a subiculum network model. J Neurosci: Off J Soc Neurosci. 2016;36:11619–33.

26. Tyzio R, Nardou R, Ferrari DC, Tsintsadze T, Shahrokhi A, Eftekhari S, et al. Oxytocin-mediated GABA inhibition during delivery attenuates autism pathogenesis in rodent offspring. Science 2014;343:675–9.

27. Chevy Q, Heubl M, Goutierre M, Backer S, Moutkine I, Eugene E, et al. KCC2 gates activity-driven AMPA receptor traffic through cofilin phosphorylation. J Neurosci: Off J Soc Neurosci. 2015;35:15772–86.

28. Gauvain G, Chamma I, Chevy Q, Cabezas C, Irinopoulou T, Bodrug N, et al. The neuronal K-Cl cotransporter KCC2 influences postsynaptic AMPA receptor content and lateral diffusion in dendritic spines. Proc Natl Acad Sci. 2011;108:15474–9.

29. Li H, Khirug S, Cai C, Ludwig A, Blaesse P, Kolikova J, et al. KCC2 interacts with the dendritic cytoskeleton to promote spine development. Neuron 2007;56:1019–33.

30. Llano O, Smirnov S, Soni S, Golubtsov A, Guillemin I, Hotulainen P, et al. KCC2 regulates actin dynamics in dendritic spines via interaction with beta-PIX. J cell Biol. 2015;209:671–86.

31. Chevy Q, Simonnet C, Al Awabdh S, Lévi S, Poncer JC. Chapter 7-Transport-dependent and independent functions of KCC2 at excitatory synapses. In: Tang X, editor Neuronal Chloride Transporters in Health and Disease. Academic Press; 2020. 133–58.

32. Goutierre M, Al Awabdh S, Donneger F, Francois E, Gomez-Dominguez D, Irinopoulou T, et al. KCC2 regulates neuronal excitability and hippocampal activity via interaction with Task-3 Channels. Cell Rep. 2019;28:91–103.e7.

33. Buzsaki G. Hippocampal sharp wave-ripple: A cognitive biomarker for episodic memory and planning. Hippocampus 2015;25:1073–188.

34. Nicoll RA. A brief history of long-term potentiation. Neuron 2017;93:281–90.

35. Whitlock JR, Heynen AJ, Shuler MG, Bear MF. Learning induces long-term potentiation in the hippocampus. Science 2006;313:1093–7.

36. Colgin LL. Rhythms of the hippocampal network. Nat Rev Neurosci. 2016;17:239–49.

37. Bortone D, Polleux F. KCC2 expression promotes the termination of cortical interneuron migration in a voltage-sensitive calcium-dependent manner. Neuron 2009;62:53–71.

38. Fellmann C, Hoffmann T, Sridhar V, Hopfgartner B, Muhar M, Roth M, et al. An optimized microRNA backbone for effective single-copy RNAi. Cell Rep. 2013;5:1704–13.

39. Chamma I, Heubl M, Chevy Q, Renner M, Moutkine I, Eugene E, et al. Activity-dependent regulation of the K/Cl transporter KCC2 membrane diffusion, clustering, and function in hippocampal neurons. J Neurosci: Off J Soc Neurosci. 2013;33:15488–503.

40. Kokare DM, Shelkar GP, Borkar CD, Nakhate KT, Subhedar NK. A simple and inexpensive method to fabricate a cannula system for intracranial injections in rats and mice. J Pharm Toxicol Methods. 2011;64:246–50.

41. Bokil H, Andrews P, Kulkarni JE, Mehta S, Mitra PP. Chronux: a platform for analyzing neural signals. J Neurosci methods. 2010;192:146–51.

42. Navas-Olive A, Valero M, Jurado-Parras T, de Salas-Quiroga A, Averkin RG, Gambino G, et al. Multimodal determinants of phase-locked dynamics across deep-superficial hippocampal sublayers during theta oscillations. Nat Commun. 2020;11:2217.

43. Colgin LL, Denninger T, Fyhn M, Hafting T, Bonnevie T, Jensen O, et al. Frequency of gamma oscillations routes flow of information in the hippocampus. Nature 2009;462:353–7.

44. Legéndy CR, Salcman M. Bursts and recurrences of bursts in the spike trains of spontaneously active striate cortex neurons. J Neurophysiol. 1985;53:926–39.

45. Ceccom J, Halley H, Daumas S, Lassalle JM. A specific role for hippocampal mossy fiber's zinc in rapid storage of emotional memories. Learn Mem. 2014;21:287–97.

46. Daumas S, Halley H, Francés B, Lassalle JMEncoding. consolidation, and retrieval of contextual memory: differential involvement of dorsal CA3 and CA1 hippocampal subregions. Learn Mem. 2005;12:375–82.

47. Hubner CA, Stein V, Hermans-Borgmeyer I, Meyer T, Ballanyi K, Jentsch TJ. Disruption of KCC2 reveals an essential role of K-Cl cotransport already in early synaptic inhibition. Neuron 2001;30:515–24.

48. Uvarov P, Ludwig A, Markkanen M, Pruunsild P, Kaila K, Delpire E, et al. A novel N-terminal isoform of the neuron-specific K-Cl cotransporter KCC2. J Biol Chem. 2007;282:30570–6.

49. Barker GR, Warburton EC. When is the hippocampus involved in recognition memory? J Neurosci: Off J Soc Neurosci. 2011;31:10721–31.

50. Vogel-Ciernia A, Wood MA. Examining object location and object recognition memory in mice. Curr Protoc Neurosci. 2014;69:8.31.

51. Phillips RG, LeDoux JE. Differential contribution of amygdala and hippocampus to cued and contextual fear conditioning. Behav Neurosci. 1992;106:274–85.

52. Gulyas AI, Sik A, Payne JA, Kaila K, Freund TF. The KCl cotransporter, KCC2, is highly expressed in the vicinity of excitatory synapses in the rat hippocampus. Eur J Neurosci. 2001;13:2205–17.

53. Otsu Y, Donneger F, Schwartz EJ, Poncer JC. Cation-chloride cotransporters and the polarity of GABA signalling in mouse hippocampal parvalbumin interneurons. J Physiol. 2020;598:1865–80.

54. White MD, Milne RV, Nolan MF. A molecular toolbox for rapid generation of viral vectors to up- or down-regulate neuronal gene expression in vivo. Front Mol Neurosci. 2011;4:8.

55. Dimidschstein J, Chen Q, Tremblay R, Rogers SL, Saldi GA, Guo L, et al. A viral strategy for targeting and manipulating interneurons across vertebrate species. Nat Neurosci. 2016;19:1743–49.

56. Boyce R, Glasgow SD, Williams S, Adamantidis A. Causal evidence for the role of REM sleep theta rhythm in contextual memory consolidation. Science 2016;352:812–6.

57. Buzsaki G. Theta oscillations in the hippocampus. Neuron 2002;33:325–40.

58. Girardeau G, Benchenane K, Wiener SI, Buzsaki G, Zugaro MB. Selective suppression of hippocampal ripples impairs spatial memory. Nat Neurosci. 2009;12:1222–3.

59. Adamantidis AR, Gutierrez Herrera C, Gent TC. Oscillating circuitries in the sleeping brain. Nat Rev Neurosci. 2019;20:746–62.

60. Colgin LL. Theta-gamma coupling in the entorhinal-hippocampal system. Curr Opin Neurobiol. 2015;31:45–50.

61. Gan J, Weng SM, Pernia-Andrade AJ, Csicsvari J, Jonas P. Phase-locked inhibition, but not excitation, underlies hippocampal ripple oscillations in awake mice in vivo. Neuron 2017;93:308–14.

62. Valero M, Cid E, Averkin RG, Aguilar J, Sanchez-Aguilera A, Viney TJ, et al. Determinants of different deep and superficial CA1 pyramidal cell dynamics during sharp-wave ripples. Nat Neurosci. 2015;18:1281–90.

63. Amilhon B, Huh CY, Manseau F, Ducharme G, Nichol H, Adamantidis A, et al. Parvalbumin interneurons of hippocampus tune population activity at theta frequency. Neuron 2015;86:1277–89.

64. Pellegrino C, Gubkina O, Schaefer M, Becq H, Ludwig A, Mukhtarov M, et al. Knocking down of the KCC2 in rat hippocampal neurons increases intracellular chloride concentration and compromises neuronal survival. J Physiol. 2011;589:2475–96.

65. Levesque M, Salami P, Shiri Z, Avoli M. Interictal oscillations and focal epileptic disorders. Eur J Neurosci. 2018;48:2915–27.

66. Menendez de la Prida L, Trevelyan AJ. Cellular mechanisms of high frequency oscillations in epilepsy: on the diverse sources of pathological activities. Epilepsy Res. 2011;97:308–17.

67. Iwasaki S, Ikegaya Y. Contextual fear memory retrieval is vulnerable to hippocampal noise. Cereb Cortex. 2021;31:785–94.

68. Tian F, Qiu Y, Lan X, Li M, Yang H, Gao Z. A small-molecule compound selectively activates K2P Channel TASK-3 by acting at two distant clusters of residues. Mol Pharm. 2019;96:26–35.

69. Wright PD, Veale EL, McCoull D, Tickle DC, Large JM, Ococks E, et al. Terbinafine is a novel and selective activator of the two-pore domain potassium channel TASK3. Biochem Biophys Res Commun. 2017;493:444–50.

70. Kourdougli N, Pellegrino C, Renko JM, Khirug S, Chazal G, Kukko-Lukjanov TK, et al. Depolarizing GABA contributes to glutamatergic network rewiring in epilepsy. Ann Neurol. 2017;81:251–65.

71. Munakata M, Watanabe M, Otsuki T, Nakama H, Arima K, Itoh M, et al. Altered distribution of KCC2 in cortical dysplasia in patients with intractable epilepsy. Epilepsia 2007;48:837–44.

72. Palma E, Amici M, Sobrero F, Spinelli G, Di Angelantonio S, Ragozzino D, et al. Anomalous levels of Cl- transporters in the hippocampal subiculum from temporal lobe epilepsy patients make GABA excitatory. Proc Natl Acad Sci USA. 2006;103:8465–8.

73. Blauwblomme T, Dossi E, Pellegrino C, Goubert E, Iglesias BG, Sainte-Rose C, et al. Gamma-aminobutyric acidergic transmission underlies interictal epileptogenicity in pediatric focal cortical dysplasia. Ann Neurol. 2019;85:204–17.

74. Woo NS, Lu J, England R, McClellan R, Dufour S, Mount DB, et al. Hyperexcitability and epilepsy associated with disruption of the mouse neuronal-specific K-Cl cotransporter gene. Hippocampus 2002;12:258–68.

75. Kelley MR, Cardarelli RA, Smalley JL, Ollerhead TA, Andrew PM, Brandon NJ, et al. Locally reducing KCC2 activity in the hippocampus is sufficient to induce temporal lobe epilepsy. EBioMedicine 2018;32:62–71.

76. Tornberg J, Voikar V, Savilahti H, Rauvala H, Airaksinen MS. Behavioural phenotypes of hypomorphic KCC2-deficient mice. The. Eur J Neurosci. 2005;21:1327–37.

77. Bliss TV, Collingridge GL. A synaptic model of memory: long-term potentiation in the hippocampus. Nature 1993;361:31–9.

78. Kim WB, Cho JH. Encoding of discriminative fear memory by input-specific LTP in the Amygdala. Neuron 2017;95:1129–46.e5.

79. Nabavi S, Fox R, Proulx CD, Lin JY, Tsien RY, Malinow R. Engineering a memory with LTD and LTP. Nature 2014;511:348–52.

80. Wulff P, Ponomarenko AA, Bartos M, Korotkova TM, Fuchs EC, Bähner F, et al. Hippocampal theta rhythm and its coupling with gamma oscillations require fast inhibition onto parvalbumin-positive interneurons. Proc Natl Acad Sci. 2009;106:3561–66.

81. Csicsvari J, Jamieson B, Wise KD, Buzsáki G. Mechanisms of gamma oscillations in the hippocampus of the behaving rat. Neuron 2003;37:311–22.

82. Hasselmo ME. What is the function of hippocampal theta rhythm? –Linking behavioral data to phasic properties of field potential and unit recording data. Hippocampus 2005;15:936–49.

83. Schlingloff D, Kali S, Freund TF, Hajos N, Gulyas AI. Mechanisms of sharp wave initiation and ripple generation. J Neurosci: Off J Soc Neurosci. 2014;34:11385–98.

84. Fernández-Ruiz A, Oliva A, Fermino de Oliveira E, Rocha-Almeida F, Tingley D, Buzsáki G. Long-duration hippocampal sharp wave ripples improve memory. Science 2019;364:1082–86.

85. Seja P, Schonewille M, Spitzmaul G, Badura A, Klein I, Rudhard Y, et al. Raising cytosolic Cl- in cerebellar granule cells affects their excitability and vestibulo-ocular learning. EMBO J. 2012;31:1217–30.

86. Pfeiffer BE. The content of hippocampal "replay". Hippocampus 2020;30:6–18.

87. Bakker A, Krauss GL, Albert MS, Speck CL, Jones LR, Stark CE, et al. Reduction of hippocampal hyperactivity improves cognition in amnestic mild cognitive impairment. Neuron 2012;74:467–74.

88. Koh MT, Haberman RP, Foti S, McCown TJ, Gallagher M. Treatment strategies targeting excess hippocampal activity benefit aged rats with cognitive impairment. Neuropsychopharmacol: Off Publ Am Coll Neuropsychopharmacol. 2010;35:1016–25.

89. Wilson IA, Ikonen S, Gallagher M, Eichenbaum H, Tanila H. Age-associated alterations of hippocampal place cells are subregion specific. J Neurosci: Off J Soc Neurosci. 2005;25:6877–86.

90. Gagnon M, Bergeron MJ, Lavertu G, Castonguay A, Tripathy S, Bonin RP, et al. Chloride extrusion enhancers as novel therapeutics for neurological diseases. Nat Med. 2013;19:1524–8.

ACKNOWLEDGEMENTS

FUNDING

AUTHOR CONTRIBUTIONS

CS, SD, and JCP designed the research; CS and MS performed the experiments; CS, MS, and MG analyzed the data; MS and MG wrote the MATLAB codes for data analysis; IM designed vectors for virus production; SD and JCP supervised the research; CS and JCP prepared the figures and wrote the manuscript with inputs from M.S., M.G. and S.D.

COMPETING INTERESTS

The authors declare no conflict of interest.

ADDITIONAL INFORMATION

Supplementary information The online version contains supplementary material available at https://doi.org/10.1038/s41386-022-01480-5.

Correspondence and requests for materials should be addressed to Jean Christophe Poncer.

Reprints and permission information is available at http://www.nature.com/reprints

Publisher's note Springer Nature remains neutral with regard to jurisdictional claims in published maps and institutional affiliations.